Neurobiology of Disease 76 (2015) 1–12

Contents lists available at ScienceDirect

Neurobiology of Disease

journal homepage: www.elsevier.com/locate/ynbdi

Frataxin knockdown in human astrocytes triggers cell death and the release of factors that cause neuronal toxicity

Frida Loría [a], Javier Díaz-Nido [a,b,c,*]

[a] Centro de Biología Molecular Severo Ochoa, CSIC-UAM, Madrid, Spain
[b] Departamento de Biología Molecular, Universidad Autónoma de Madrid, Madrid, Spain
[c] Center for Biomedical Research on Rare Diseases (CIBERER), Madrid, Spain

ARTICLE INFO

Article history:
Received 10 July 2014
Revised 15 November 2014
Accepted 21 December 2014
Available online 29 December 2014

Keywords:
Friedreich's ataxia
Astrocytes
Cell death
Apoptosis
Neurotoxicity
Neurodegeneration

ABSTRACT

Friedreich's ataxia (FA) is a recessive, predominantly neurodegenerative disorder caused in most cases by mutations in the first intron of the frataxin (FXN) gene. This mutation drives the expansion of a homozygous GAA repeat that results in decreased levels of FXN transcription and frataxin protein. Frataxin (Fxn) is a ubiquitous mitochondrial protein involved in iron–sulfur cluster biogenesis, and a decrease in the levels of this protein is responsible for the symptoms observed in the disease. Although the pathological manifestations of FA are mainly observed in neurons of both the central and peripheral nervous system, it is not clear if changes in non-neuronal cells may also contribute to the pathogenesis of FA, as recently suggested for other neurodegenerative disorders. Therefore, the aims of this study were to generate and characterize a cell model of Fxn deficiency in human astrocytes (HAs) and to evaluate the possible involvement of non-cell autonomous processes in FA. To knockdown frataxin *in vitro*, we transduced HAs with a specific shRNA lentivirus (shRNA37), which produced a decrease in both frataxin mRNA and protein expression, along with mitochondrial superoxide production, and signs of p53-mediated cell cycle arrest and apoptotic cell death. To test for non-cell autonomous interactions we cultured wild-type mouse neurons in the presence of frataxin-deficient astrocyte conditioned medium, which provoked a delay in the maturation of these neurons, a decrease in neurite length and enhanced cell death. Our findings confirm a detrimental effect of frataxin silencing, not only for astrocytes, but also for neuron–glia interactions, underlining the need to take into account the role of non-cell autonomous processes in FA.

Introduction

Friedreich's ataxia (FA) is a hereditary disorder caused in most cases by the expansion of GAA repeats in the first intron of the frataxin (FXN) gene, which dampens the expression of frataxin (Fxn), a protein involved in the biogenesis of iron–sulfur clusters and the regulation of oxidative stress (Campuzano et al., 1996; Campuzano et al., 1997; Pastore and Puccio, 2013). FA is characterized by progressive neurodegeneration that mainly affects the dorsal root ganglia, the corticospinal and spinocerebellar tracts of the spinal cord, and the deep cerebellar nuclei (Delatycki and Corben, 2012; Koeppen and Mazurkiewicz, 2013). Until recently, neurodegenerative diseases have been regarded as exclusively neuronal disorders and the contribution of non-neuronal cells to FA has been largely ignored. However, there is now considerable evidence that the selective death of certain types of neurons is not only due to intrinsic changes within the vulnerable neurons but also, to additional changes within neighboring non-neuronal glial cells (Verkhratsky et al., 2012). Indeed, non-cell autonomous mechanisms mediated by glial dysfunction appear to contribute to the vulnerability of neurons in many neurodegenerative diseases (Liu et al., 2005; Ilieva et al., 2009; Lu et al., 2009; Rodriguez and Verkhratsky, 2011; Tao et al., 2011; Di Malta et al., 2012; Garden and La Spada, 2012; Meyer et al., 2014). In the case of FA, specific silencing of Fxn in glial cells triggers a phenotype in *Drosophila* similar to that observed after ubiquitous Fxn reduction, characterized by altered lipid metabolism in glial cells, degeneration of neurons, severely impaired locomotor activity and reduced lifespan (Navarro et al., 2010). Thus, it seems plausible that non-cell autonomous processes might contribute to neurodegeneration in FA.

Astrocytes are the most abundant glial cell type in the central nervous system (CNS), and fulfill a wide variety of complex and essential functions responsible for maintaining brain homeostasis (Barres, 2008; Belanger et al., 2011), such as: controlling fluid movement between the intracellular and extracellular space; protecting neurons against oxidative stress; regulating energy metabolism and blood flow; and modulating neuronal activity through the expression of cytokines, growth factors and transporters (Sofroniew and Vinters, 2010; Allaman et al., 2011). These cells are crucial for the correct functioning

Abbreviations: FA, Friedreich's ataxia; Fxn, frataxin; HAs, human astrocytes; shRNA, short hairpin RNA; ACM, astrocyte conditioned medium.

* Corresponding author at: Centro de Biología Molecular Severo Ochoa (CBMSO), Universidad Autónoma de Madrid, Campus de Cantoblanco, C/Nicolás Cabrera 1, 28049 Madrid, Spain. Fax: +34 911964420.
E-mail address: javier.diaznido@uam.es (J. Díaz-Nido).

Available online on ScienceDirect (www.sciencedirect.com).

http://dx.doi.org/10.1016/j.nbd.2014.12.017
0969-9961/

of neurons, microglia, oligodendrocytes and endothelial cells. Nevertheless, while the functional effects of Fxn depletion in neurons have been studied to some extent (Palomo et al., 2011; Mincheva-Tasheva et al., 2014), less is known about the consequences of Fxn loss in astrocytes. Using an *in vitro* approach, we have characterized the effects of Fxn depletion in cultured human astrocytes (HAs). Accordingly, we describe the detrimental effects of Fxn deficiency in astrocytes, and we provide evidence that this astrocyte dysfunction has a negative impact on neuronal maturation and survival. Therefore, our results provide evidence of the crucial contribution of non-cell autonomous glial interactions in the neurodegeneration observed in FA.

Materials and methods

Lentiviral production and titration

To establish an *in vitro* model of Fxn knockdown in human astrocytes, lentiviral vectors expressing short hairpin RNA (shRNA) sequences were purchased from Sigma-Aldrich (Madrid, Spain) and they contained either the sequences against the human FXN gene (shRNA37: Mission® shRNA, Gene Bank accession number NM_000144), or a non-specific scrambled control (SCR: Mission® Non-Target shRNA, SHC002). Lentiviral packaging, stock production and titration was performed as described previously (Follenzi and Naldini, 2002).

Cell cultures

Human astrocyte cultures

Primary human astrocytes (HAs: generously donated by Dr. Vega García-Escudero and Dr. Filip Lim, Centro de Biología Molecular Severo Ochoa, Madrid, Spain) were obtained from ScienCell Research Laboratories (Cat no 1800; Carlsbad, CA, USA). The cells were cultured in astrocyte medium (Sciencell Cat no 1801) in 2 μg/cm^2 poly-L-lysine-coated (PLL: Sigma-Aldrich) 100 mm culture dishes and handled according to the manufacturer's recommendations. Before any experimentation started, the HAs were characterized by immunostaining for two well-known astrocyte markers: rabbit anti-GFAP (1:500; Promega Biotech, Madrid, Spain) and mouse anti-S100β (1:1000; Sigma-Aldrich). Confluent cells were detached in 0.25% Trypsin/0.5 mM ethylenediaminetetraacetic acid (EDTA), and they were seeded in 60 mm dishes or in multi-well plates (with or without glass coverslips) at a density between 5000 and 7500 cells/cm^2. The cells were left in medium for at least 2 days *in vitro* (DIV) and then transduced with the lentiviral vectors or left as controls.

Astrocyte conditioned medium (ACM)

Conditioned medium from HAs was prepared as described previously, with some modifications (Lafon-Cazal et al., 2003). Equal number of cells were plated in astrocyte medium and transduced with SCR or shRNA37 lentiviral vectors. After 48 h, the medium was replaced with neuronal medium and after a further 48 h, ACM was collected at 96 h post transduction. Upon collection, the ACM was centrifuged twice to eliminate cell debris, filtered and frozen at −20 °C.

Primary neuronal cultures

Primary cortical neurons were prepared from C57BL/6 mice (embryonic days 16–18), as described previously (Tapia et al., 2010). Briefly, pregnant mice were sacrificed by cervical dislocation, the fetuses were removed and decapitated, and the meninges were stripped off the exposed brain. The cortices were removed and digested in trypsin (0.25%: Life Technologies, Madrid, Spain) containing DNaseI (1 mg/ml: Roche Diagnostics, Madrid, Spain) for 15 min at 37 °C, and then dissociated by trituration with a fire-polished Pasteur pipette. The dissociated cortical cells were plated in multiwell dishes previously coated with PLL (1 mg/mL) or on PLL-coated coverslips, and maintained in Neurobasal® medium (Life Technologies) supplemented with 10% horse serum at densities ranging from 40,000 to 60,000 cells/cm^2. To analyze the possible effects of conditioned medium from Fxn-depleted astrocytes on neuronal growth and maturation, the medium was changed after 3 h to either neuronal medium (Neurobasal medium supplemented with B-27® [Life Technologies], Glutamax™ [Life Technologies] and penicillin/streptomycin) or to ACM. The cells were then incubated at 37 °C in a humidified atmosphere containing 5% CO_2.

Cell viability

Cell viability was quantified by measuring calcein acetoxymethyl ester/propidium iodide (calcein/PI) uptake (Mattson et al., 1995). In living cells, the non-fluorescent calcein is converted to a green-fluorescent calcein after acetoxymethyl ester hydrolysis by intracellular esterases, while non-viable cells can be distinguished by a bright red fluorescence emitted when PI intercalates into double-stranded nucleic acid in cells with a disrupted plasma membranes. Briefly, cells were incubated at 37 °C for 20 min with 1 μM of Calcein AM (Molecular Probes, Life Technologies) and 4 μM of PI (Sigma-Aldrich), and they were then visualized on an Axiovert 200 fluorescence inverted microscope (Zeiss). Three randomly selected fields were captured and analyzed per experimental condition, and the experiments were performed in duplicate on three independent cultures. Cell viability was calculated as the percentage of green cells relative to the total number of cells (both red and green).

Protein extraction and western blots

Following treatment, the cells were rinsed once with phosphate buffer saline (PBS) and homogenized in lysis buffer: 20 mM 4-(2-hydroxyethyl) piperazine-1-ethanesulfonic acid (HEPES), 100 mM sodium chloride (NaCl), 100 mM sodium fluoride (NaF), 1% Triton X-100, 1 mM sodium orthovanadate (Na_3VO_4), 5 mM EDTA and the COMPLETE™ protease inhibitor cocktail (Roche Diagnostics). The resulting soluble fractions were centrifuged at 16,000 × *g* for 10 min at 4 °C, and the supernatants were taken as the whole cell lysate, mixed with electrophoresis buffer and boiled for 5 min. The protein concentration was measured using the Bio-Rad DC protein assay, according to the manufacturer's instructions (Bio-Rad Laboratories, Madrid, Spain). For western blots, equal amounts of protein (10–30 μg/well) were separated on 6–15% sodium dodecyl sulfate–polyacrylamide gel electrophoresis gels (SDS–PAGE) and immobilized on nitrocellulose membranes (GE Healthcare, Barcelona, Spain), following standard procedures. The membranes were probed overnight at 4 °C with primary antibodies diluted in a blocking solution (PBS containing 0.1% Tween-20 and 5% non-fat dried milk). The membranes were then washed and exposed for 1 h at room temperature to the appropriate secondary peroxidase-conjugated antibody (1:5000), visualizing the specific protein bands by chemiluminescence. Following detection, the membranes were stripped of antibodies using a commercial kit (Restore Western Blot Stripping Buffer; Fischer Scientific, Madrid, Spain) and then re-probed for other proteins. The primary antibodies used in this study were: rabbit anti-Frataxin (1:1000; clone H155; Santa Cruz Biotechnology, Heidelberg, Germany), goat anti-cyclin-dependent kinase inhibitor 1A; p21 (1:1000; Santa Cruz Biotechnology), mouse anti-p53 (1:1000; DO-7; BD Biosciences, Madrid, Spain), rabbit anti-Caspase-3 (1:500; #9662; Cell Signaling, Boston, MA, USA). The western blots were quantified by densitometry using NIH ImageJ (Bethesda, MD, USA) open source software and the absolute values (arbitrary units) from each experimental group were normalized to those obtained for mouse anti-β-actin (1:5000; Sigma-Aldrich) used as a control for loading. The results are presented in arbitrary units expressed as the change relative to their respective controls that were run simultaneously.

Mitochondrial superoxide production

The superoxide anions within mitochondria were measured by flow cytometry with the MitoSOX™ Red probe (Molecular Probes, Life Technologies) following a previously described protocol (Mukhopadhyay et al., 2007). The astrocyte medium was removed from the culture plates 96 h after shRNA37 transduction and it was replaced with medium containing 5 μM MitoSOX™ Red, in which the cells were incubated for 30 min. While minimizing their exposure to light, the cells were recovered by trypsinization and centrifuged at 1000 rpm for 5 min. The pellets were washed twice with Hank's balanced salt solution (HBSS; Life Technologies) and re-suspended in 500 μl of Mitochondria Incubation Buffer (MIB: 68 mM sucrose, 10 mM HEPES [pH 7.4], 70 mM potassium chloride [KCl], 1 mM ethylene glycol tetraacetic acid [EGTA]: all from Sigma-Aldrich). As a positive control, 10 μM of the apoptosis-inducing agent Antimycin A (Sigma-Aldrich) was added to the cells. Subsequently, the cell suspensions were transferred to cytometry tubes and analyzed in a FACSCanto II flow cytometer (BD Biosciences) with 488 nm excitation, measuring MitoSOX™ red in the FL2/3 channels and collecting at least ≥15,000 events per condition. To measure oxidized MitoSOX in HAs data were collected and plotted for forward (FSC) vs side (SSC) scatter to exclude the artifactual oxidation of necrotic cells to the overall oxidation measurements. The results were examined using the FlowJo software by plotting each population as a histogram of mean intensity (FL2). Experiments were performed in triplicate and the data represent the geometric mean ± S.E.M. of three independent experiments.

Human antibody-based protein arrays of astrocyte conditioned medium

Equivalent numbers of human astrocytes were cultured in complete astrocyte medium and transduced with SCR or shRNA37 lentiviral vectors. The medium was changed to serum-free astrocyte medium 48 h after transduction and collected after a further 48 h. The secretome of HAs was analyzed with the RayBio® Human Cytokine Antibody Array C series 1000 kit (RayBiotech, Inc., Norcross, GA, USA) according to the manufacturer's instructions. The assay membranes can detect 120 different growth factors and cytokines at a time. Briefly, each membrane was placed into the 8-well tray provided, and it was incubated at room temperature in 2 mL of the blocking buffer provided for 30 min. The blocking buffer was decanted and the membranes were incubated overnight with 1 mL of media from SCR or Fxn-depleted human astrocytes at 4 °C. After removing the media, the containers were washed 3 times with 2 mL of wash buffer I at room temperature with shaking for 5 min and they were then washed twice more with 2 mL of wash buffer II at room temperature with shaking for 5 min. The membranes were probed overnight at 4 °C with 1 mL of diluted primary biotin-conjugated antibody, and after washing with wash buffer I and II, antibody binding to the membranes was detected by incubation with 2 mL of 1000-fold diluted HRP-conjugated streptavidin at room temperature for 2 h. The membranes were again washed twice and placed into the visualization buffer. Excess visualization reagent was drained off and the membranes were covered with a clean piece of plastic. Antibody binding was visualized by chemiluminescence in an ImageQuant™ LAS 4000 mini imaging system (GE Healthcare) and the spots detected were quantified by the apparatus. After blank subtraction, the data were normalized to the positive controls provided by the manufacturer and the results are expressed as mean fold change ± S.E.M. of SCR condition.

Sample collection and RNA extraction

After treatment, the cells were washed once with PBS, frozen on dry ice and stored at −80 °C. For reverse transcription-polymerase chain reaction (RT-PCR), total RNA was extracted using RNeasy mini columns (Qiagen, Hilden, Germany) and any contaminating genomic DNA was eliminated by DNaseI (Qiagen) digestion. The yield and purity of the RNA was determined using a Nanodrop spectrophotometer (Nanodrop Technologies, Wilmington, DE, USA).

Reverse transcription and quantitative PCR (qPCR)

Total RNA (0.5 μg in 20 μL) was reverse transcribed into cDNA (25 ng/μl final concentration), using the Super Script III First Strand Synthesis SuperMix kit for qPCR (Invitrogen, Life Technologies), with a mix of random and oligo(dT) primers. Primers (human) were designed from previously published sequences or in house (Table 1) and to avoid genomic DNA amplification, the primers were designed to span intron–exon boundaries (all from Sigma-Aldrich). For FXN, PIGF, HGF, IGFBP-3, IL-6 and VPA genes, qPCR was performed on 2.5 ng of cDNA with the SsoFast EvaGreen supermix (BioRad Laboratories) with 500 nM primers and using the CFX 384 system (BioRad Laboratories) with cycling conditions of: 95 °C for 5 s; 40 cycles of 95 °C for 5 s + 60 °C for 5 s; and 60 °C for 5 s + 95 °C for 5 s. In the case of MIP-1α, qPCR was performed from 25 ng of cDNA using the Power SYBR Green PCR Master Mix (Applied Biosystems, Life Technologies) with 250 nM primers and using the 7900HT Fast system (Applied Biosystems, Life Technologies) with cycling conditions of: 95 °C for 10 s; 40 cycles of 95 °C for 15 s + 60 °C for 60 s; and 95 °C for 15 s + 60 °C for 15 s + 95 °C for 15 s. To ensure the absence of possible genomic DNA contamination, we used the ValidPrime method (Laurell et al., 2012), measuring the genomic DNA content in RT(+) samples with commercially available reference samples and primers (ValidPrime™, TATAA Biocenter, Sweden). The data were analyzed and corrected (where necessary) with the GenEx software. Glyceraldehyde-3-phosphate dehydrogenase (GAPDH) expression was used to normalize the data and to obtain relative expression values with the comparative Ct method. The results are expressed as the fold-change compared to SCR HAs ± S.E.M. of three independent cultures measured in triplicate.

Immunocytochemistry and optical/confocal microscopy

Immunostaining of cells was performed following our previously described procedures (Loria et al., 2010). Cells plated on PLL-coated coverslips were fixed in 4% paraformaldehyde for 10 min and non-specific binding was blocked with 2% bovine serum albumin (Sigma-Aldrich) in PBS containing 0.1% Triton X-100. The cells were then incubated overnight at 4 °C with the primary antibodies mouse anti-SMI31 (1:1000; Covance, Princeton, NY, USA) and rabbit polyclonal anti-microtubule-associated protein 2 (1:1000, 514) (Sanchez Martin et al., 1998). After rinsing with PBS, antibody binding was detected with Alexa Fluor 488 (1:1000, goat anti-mouse IgG; Molecular Probes, Life Technologies) or Alexa Fluor 555 (1:1000, goat anti-mouse IgG; Molecular Probes, Life Technologies) secondary antibodies for 1 h at room temperature. The nuclei were counterstained with DAPI (1:5000; Calbiochem, Millipore, Madrid, Spain) and after washing, the glass coverslips were mounted on slides. Non-specific interactions of secondary antibodies were verified by omitting the primary antibodies. To visualize intact mitochondria and mitochondrial superoxide production, live cells were labeled with MitoTracker red and MitoSOX red probes, according to the manufacturer's instructions. After fixation and immunostaining, images were acquired either with an LSM710 vertical laser scanning confocal microscope (Zeiss) or with an Axiovert 200 fluorescence inverted microscope coupled to a CCD camera (Zeiss).

Neuronal quantitative analysis

To analyze neurite outgrowth and branching in primary neuronal cultures, after immunostaining with SMI31 or MAP-2, the cells were observed on a Zeiss Axiovert 200 inverted fluorescence microscope equipped with a CCD camera. For each experimental condition, at least five randomly chosen fields were captured and the axons and dendrites were traced from the cell body to the end of their prolongations,

Table 1
Primers used for SYBR Green qPCR.

Protein/gene name	Accesion no.	Primer name	Sequence (5′–3′)
Frataxin (FXN)	NM_000144	FXN-Fw	TGGAATGTCAAAAAGCAGAGTG
		FXN-Rv	CCACTCCCAAAGGAGACATC
Phosphatidylinositol glycan anchor biosynthesis (PIGF)	NM_002643.3	PIGF-Fw	TAGGACCAAACCTCAAAGCA
		PIGF-Rv	AAAGACCATGGCAGGTATGG
Hepatocyte growth factor (HGF)	NM_000601.4	HGF-Fw	TCGGGGTAAAGACCTACAGGA
		HGF-Rw	AATGGGGAGAGTTATCGAGGT
Insulin-like growth factor binding protein 3 (IGFBP-3)	NM_001013398	IGFBP3-Fw	GCCAGGAAATGCTAGTGAGTCG
		IGFBP3-Rv	GGCAGGGACCATATTCTGTCT
Interleukin 6 (IL-6)	NM_000600.3	IL-6-Fw	CACTCACCTCTTCAGAACG
		IL-6-Rv	ATTTGTGGTTGGGTCAGGG
Macrophage inflammatory protein 1 alpha (MIP-1α)	NM_002983	MIP-1α-Fw	CAACCAGTTCTCTGCATCACTTG
		MIP-1α-Rv	GCCGGGAGGTGTAGCTGAA
Glyceraldehyde-3-phosphate dehydrogenase (GAPDH)	NM_002046.4	GAPDH-Fw	CCCCTGGCCAAGGTCATCCATG
		GAPDH-Rv	CAGTGAGCTTCCCGTTCAGCTC

calculating the sum of the distance per field with the ImageJ plugin NeuronJ (Meijering et al., 2004). In the case of neuron number, the total DAPI positive cells were counted in each field and condition. For all measurements, the results were normalized to the CTL condition and they are presented as the mean percentage ± S.E.M.

Statistics

Statistical analysis was performed using the SPSS 18.0 statistical package. The results are expressed as the mean ± standard error mean (S.E.M.). Unless stated in the figure legend, the Student's t-test was used to compare between two groups. If the Levene's test for homogeneity of variances was significant then the Mann–Whitney's U non-parametric test was used. Statistical significance was attributed when $p \leq 0.05$.

Results

Reduced in vitro expression of frataxin in glial cells after shRNA-mediated knockdown

In order to determine and characterize the effects of Fxn deficiency in glial cells, and since the use of lentiviral vectors has proven to be a useful tool to study biological mechanisms (Aurelie et al., 2013), we established an *in vitro* model of Fxn knockdown through a Fxn-specific shRNA (shRNA37) lentiviral vector. First, we investigated the Fxn protein in HAs at different time points up to 96 h after the transduction of the shRNA37 vector and compared Fxn levels with those of untransduced cells (CTL) and scrambled (SCR) transduced cells at 96 h. In western blots we observed a progressive decrease in Fxn levels from 24 h post-transduction that continued falling until 96 h post-transduction when the protein levels reached approximately 24% of the control cells (Fig. 1A). Since the majority of FA patients have Fxn protein levels between 10% and 25% of normal values and our data indicated that similar levels were achieved after 96 h of transduction, we assessed the Fxn mRNA in astrocytes at this time point after shRNA37 or SCR transduction by quantitative PCR (qPCR). Fxn mRNA expression was significantly downregulated in Fxn-deficient HAs compared with the SCR transduced controls, with almost undetectable Fxn expression in those cells (Fig. 1B). Together these data confirmed that both Fxn protein and mRNA is diminished in our *in vitro* HA model of Fxn knockdown.

Mitochondrial superoxide production after frataxin silencing in human astrocytes

The negative effects of Fxn deficiency, specifically in the mitochondria, are related to the cell's redox status (Lefevre et al., 2012; Gonzalez-Cabo and Palau, 2013). Therefore, 96 h after transduction

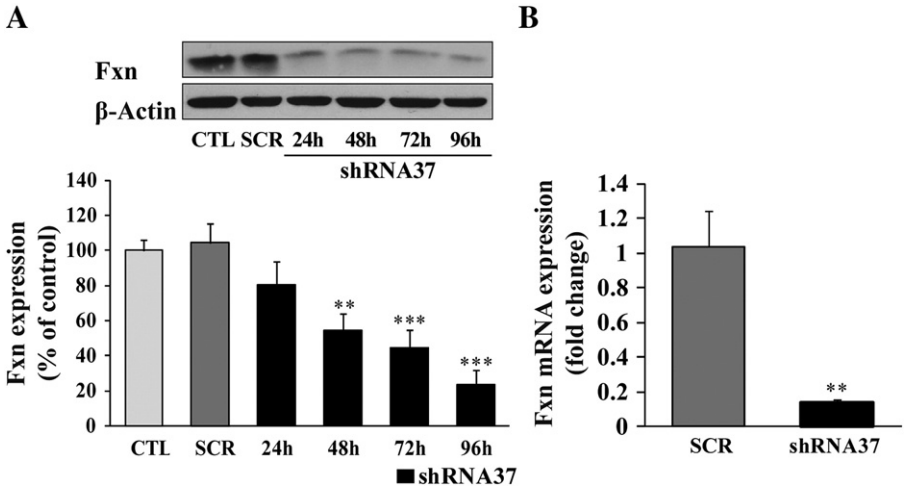

Fig. 1. Frataxin protein and mRNA expression in HAs after *in vitro* knockdown. (A) HAs were cultured under standard conditions (CTL) or transduced with SCR or shRNA37 lentivirus for the times indicated. The cells were lysed and recovered, and equal amounts of protein from these cells (15 μg/lane) were immunoblotted and probed with antibodies against Fxn and β-actin (as a loading control). The lower panel shows the quantification of the CTL (light gray bar), SCR (dark gray bar) and shRNA37-transduced (black bar) signals from HAs. All the time points were compared with CTL and SCR cells at 96 h. (B) Total mRNA was extracted from HAs 96 h after transduction with SCR (dark gray bar) or shRNA37 (black bar) lentivirus and FXN gene expression was analyzed by qPCR. FXN expression was normalized to GAPDH and the histograms show the mean values ± S.E.M. from at least three independent experiments: $^{**}p < 0.01$ and $^{***}p < 0.001$ compared to SCR.

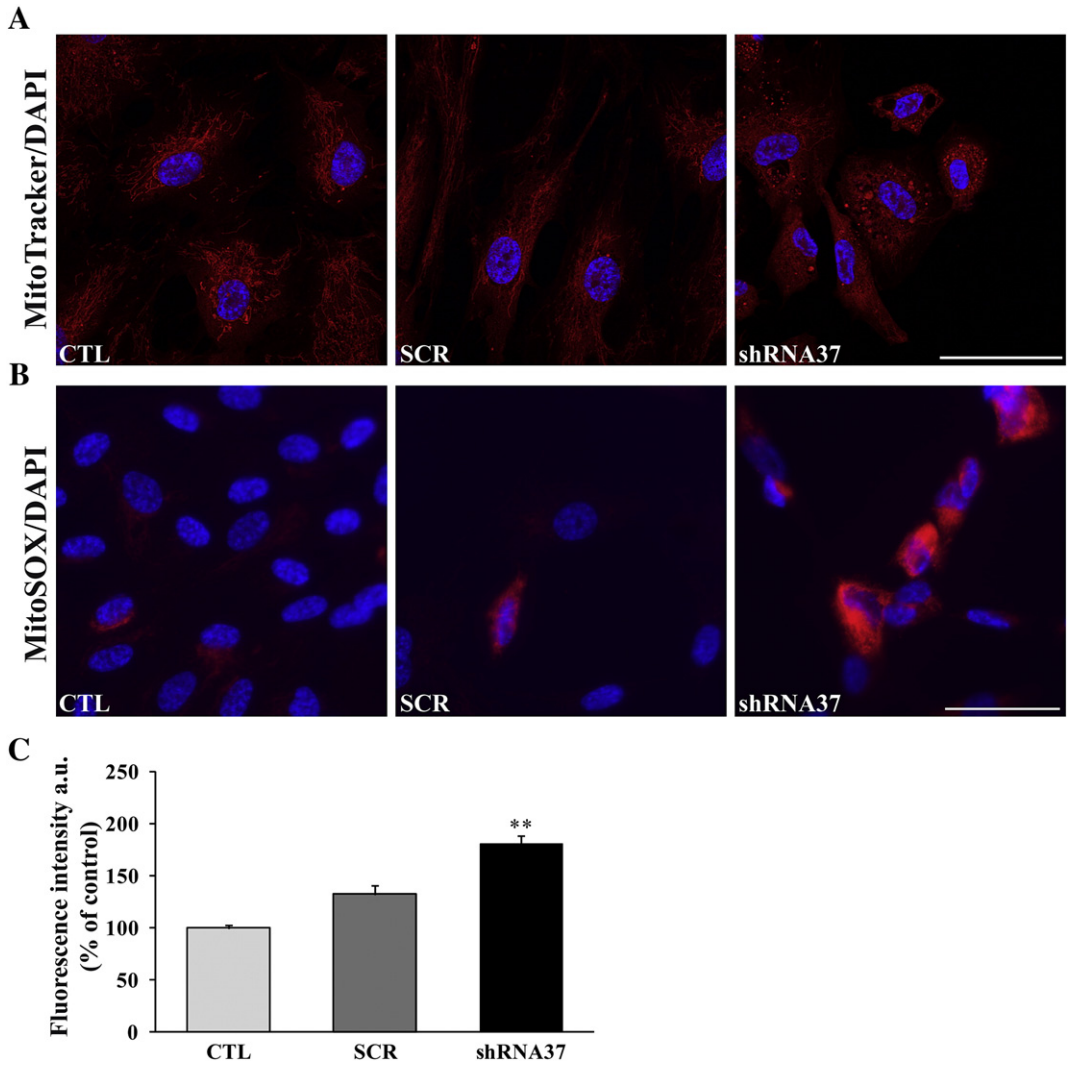

Fig. 2. Morphological changes in mitochondria and superoxide production in Fxn-depleted HAs. (A) Representative confocal photomicrographs of CTL, SCR or shRNA37-transduced HAs stained with the MitoTracker red probe. The nuclei were counterstained with DAPI (blue). (B) Fluorescence microscopy images showing representative staining of CTL, SCR or shRNA37 astrocytes after immunostaining with the MitoSOX red probe and DAPI (blue). Scale bar in (A) and (B); 50 μm. (C) Increased mitochondrial superoxide production in live astrocytes assessed with the MitoSOX red probe and by flow cytometry. The panel summarizes the flow cytometry data from three independent experiments. The bar graph represents the geometric mean ± S.E.M. (arbitrary units) of the MitoSOX fluorescence intensities of CTL (light gray bar), SCR (dark gray bar) and shRNA37-transduced HAs (black bar). Results in (A), (B) and (C) correspond to data analyzed at 96 h in all experimental conditions: $^{**}p < 0.01$ compared with SCR.

with the SCR or the shRNA37 lentivirus we evaluated both mitochondrial morphology and superoxide generation in HAs labeled with MitoTracker red and MitoSOX red probes. In terms of mitochondrial integrity evident by confocal microscopy, the typical filamentous mitochondria characteristic of control cells were replaced by severely swollen mitochondria and punctate MitoTracker staining in Fxn-deficient astrocytes (Fig. 2A). Furthermore, the weak MitoSOX fluorescence in control conditions became a strong signal in the cells lacking Fxn, reflecting superoxide formation (Fig. 2B). Thus, we evaluated the mitochondrial oxidant burden in live Fxn-deficient astrocytes tagged with the MitoSOX red probe 96 h after lentiviral vector transduction. Flow cytometry analysis showed that Fxn-deficient cells produce more superoxide than either control or SCR astrocytes measured also at 96 h (Fig. 2C), reflected by significantly more intense red MitoSOX fluorescence.

Frataxin knockdown decreases the viability and proliferation of human astrocytes

Having established our *in vitro* model of Fxn knockdown in human astrocytes, we studied whether lower levels of Fxn affected the rate of cell survival. Astrocyte viability, was measured over 96 h, evaluating cell viability every 24 h as the percentage of calcein positive cells relative to the total cell number (Fig. 3A). While no change in this parameter was observed between 24 and 48 h, shRNA37 transduction decreased HA survival to 80% at 72 h post-transduction and to 69% after 96 h (Fig. 3B). To discern if Fxn depletion induced changes in cell proliferation in addition to cell death, we tracked the total cell number (calcein/PI positive cells) over time and we found a significant reduction of the total number of cells 48, 72 and 96 h after Fxn knockdown but not in the control HAs or SCR transduced cells, the numbers of which increased progressively (Fig. 3C). This suggests that in our model, an acute decrease in Fxn levels slows down cell proliferation and induces the death of HAs.

Signs of possible cell cycle arrest and apoptosis in human astrocytes after frataxin silencing

The transcription factor p53 plays a key role in regulating events like DNA repair and the cell cycle (Jebelli et al., 2012). Moreover, p53 is involved in the induction of apoptosis, particularly in a neuronal model of Fxn silencing (Palomo et al., 2011). Accordingly, we hypothesized that this protein could be involved in the cell death associated with the decreased cell proliferation and viability of HAs when Fxn was

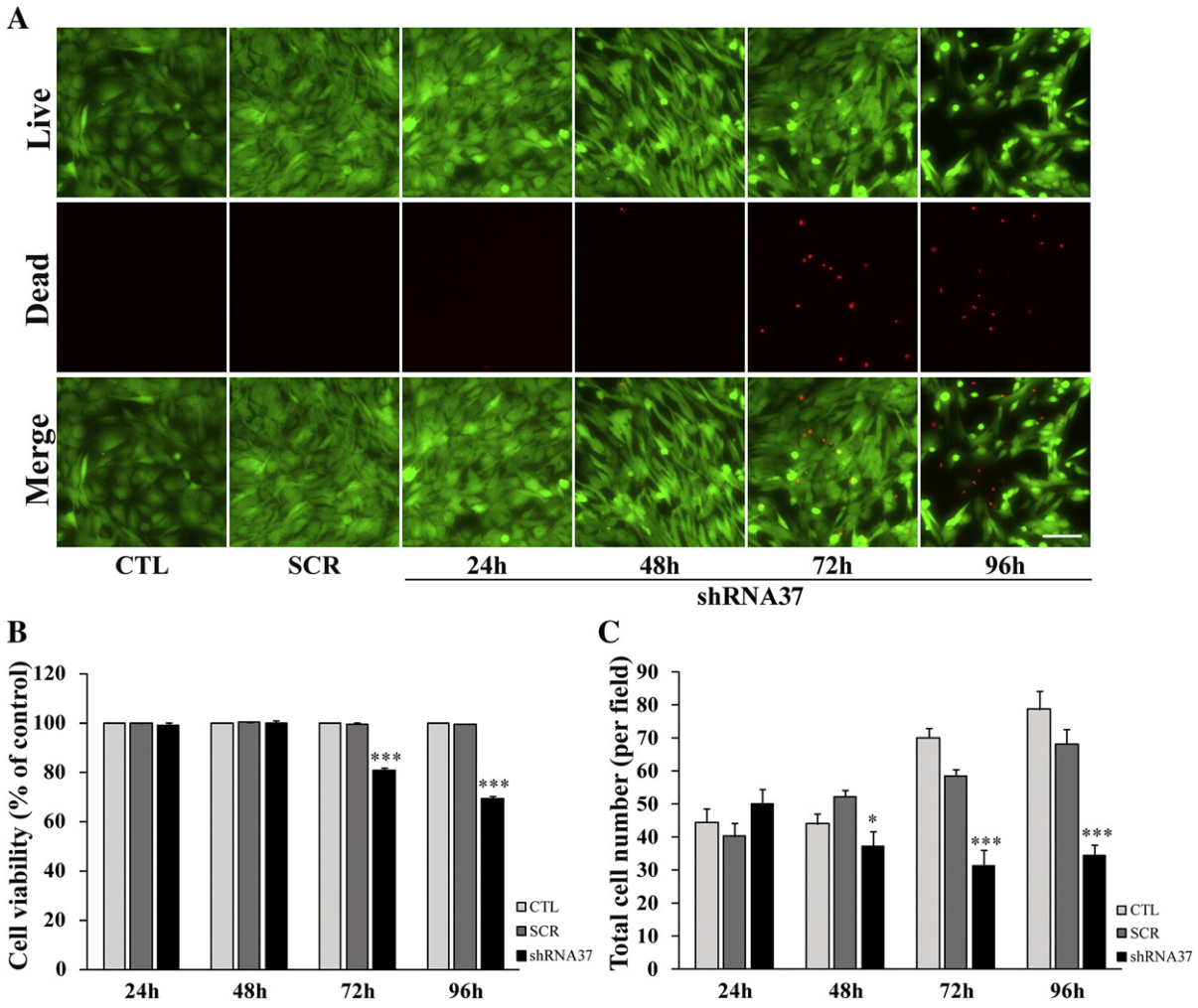

Fig. 3. Fxn knockdown in HAs decreases cell survival and proliferation. (A) Cell viability was estimated by calcein/PI uptake. Live CTL HAs or those transduced with SCR or shRNA37 were incubated with a mixture of both dyes and visualized by fluorescence microscopy at the times indicated. Representative images of the live (calcein positive, green) and dead/dying cells (PI positive, red). Scale bar: 100 μm. (B) The number of live astrocytes (green) was quantified with respect to the total cell number (green + red), and expressed as a percentage of the CTL cells at each time point. (C) Quantitative analysis of cell proliferation estimated through the total cell number in each condition over 4 DIV. The data represent the mean ± S.E.M. of at least 6 images per condition from three independent experiments: $^{*}p < 0.05$ and $^{***}p < 0.001$ compared with SCR condition. In (B) and (C): CTL, light gray bar; SCR, dark gray bar; shRNA37, black bar.

silenced. Hence, we evaluated the p53 protein in control (CTL/SCR) and Fxn-depleted HAs in western blots, and we found significantly more p53 in astrocytes lacking Fxn at all time points evaluated (Figs. 4A and D). We also measured the expression of the cyclin-dependent kinase inhibitor 1A (p21), a downstream effector of p53-mediated cell cycle arrest. As expected, from 48 h after shRNA37 transduction we detected a sustained increase of p21 expression in these cells (Figs. 4B and D). Finally, we determined whether there was any change in the well-known marker of apoptotic events, caspase-3. The lack of Fxn induced a time dependent increase in cleaved caspase-3 compared with both the control and SCR groups (Figs. 4C and D). For the 3 proteins evaluated, the time points were compared with control levels corresponding to untransduced and SCR cells collected at 96 h. These results suggest that a deficiency of Fxn in HAs triggers the activity of p53, p21 and caspase-3 (cleaved), implying that the cell death of these cells may be at least in part due to apoptosis and the activation of the p53 pathway.

Cytokine profiling of conditioned medium after frataxin silencing in human astrocytes

Given the role of glial cells in fundamental processes within the CNS, characterizing the secretome of these cells under homeostatic and pathological conditions is becoming ever more relevant (Dowling and Clynes, 2011). To examine the functional consequences of Fxn silencing in HAs in more detail, we analyzed the secretome of these cells by collecting serum-free astrocyte conditioned medium (ACM) after 48 h of conditioning (a total of 96 h after SCR or shRNA37 lentiviral transduction). Using an array that identifies up to 120 cytokines (Fig. 5A), we detected 49 cytokines with increased secretion (mild to strong), and 6 cytokines with decreased secretion in Fxn-depleted HAs (data not shown, see Fig. 5B for the most relevant findings). According to their principal functions, these cytokines were classified into the following groups: i) proliferation/angiogenesis; ii) immunity/inflammation; iii) growth factors/growth factor receptors; and iv), broad-acting cytokines (Table 2). These cytokine array results were validated at the transcriptional level by qPCR (Fig. 5C) and we detected significant increases in the mRNA expression of HGF, IGFBP-3, IL-6, PIGF and MIP-1α, with no obvious changes in GRO-α, MIF or GFBP-2 expression. For some of the genes analyzed (e.g. Angiogenin, ICAM-3 or VEGF-α), the transcriptional changes detected by qPCR were not consistent with the cytokine array data, which may reflect the influence of other post-transcriptional regulatory events (data not shown). Nevertheless, the consistent increase in the mRNA expression and secretion of HGF, IGFBP-3, IL-6, PIGF and MIP-1α provoked by Fxn-deficiency suggests a functionally relevant alteration in cell communication pathways.

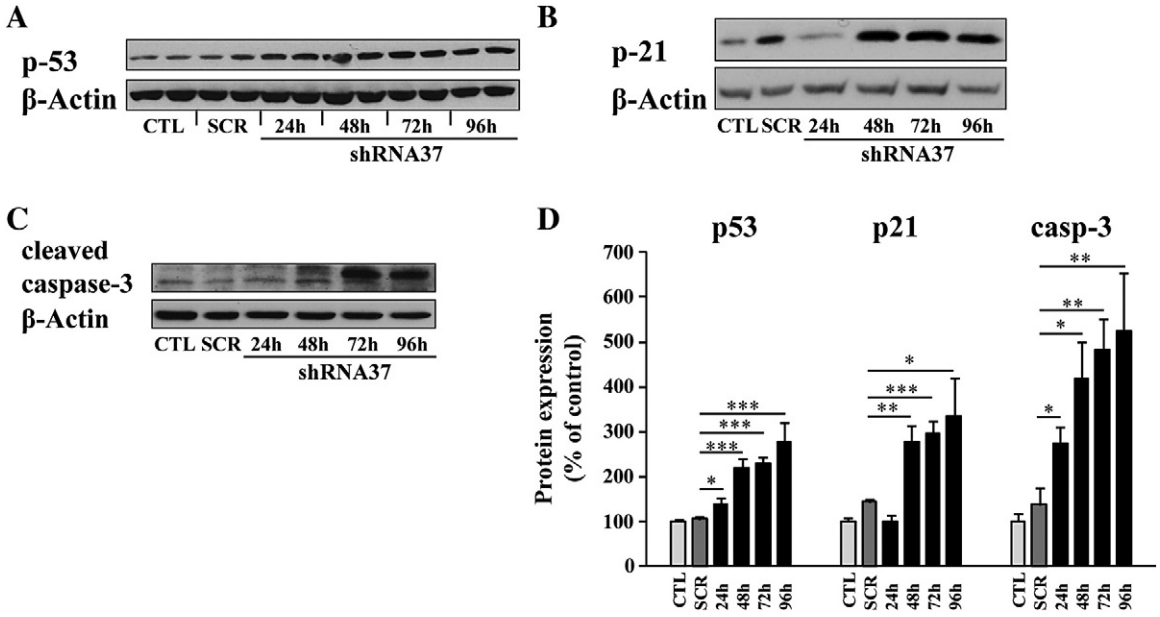

Fig. 4. Increased expression of cell cycle and apoptosis-related proteins after Fxn shRNA silencing in glial cells. Representative immunoblots of the tumor suppressor protein p53 (A), its downstream effector p21 (B), and the marker of apoptosis, cleaved caspase-3 (C). Equal amounts of protein (15–30 μg) from CTL and SCR cells collected at 96 h, and from HAs at different time points after shRNA37 transduction were resolved by SDS-PAGE (15%), immunoblotted and probed with the corresponding antibody. In all cases, β-actin was used as a loading control. (D) Quantification of (A–C), where the data represent the mean ± S.E.M. (arbitrary units) normalized to the control after densitometry of data from at least three independent experiments: $^{*}p < 0.05$, $^{**}p < 0.01$ and $^{***}p < 0.001$ compared with SCR.

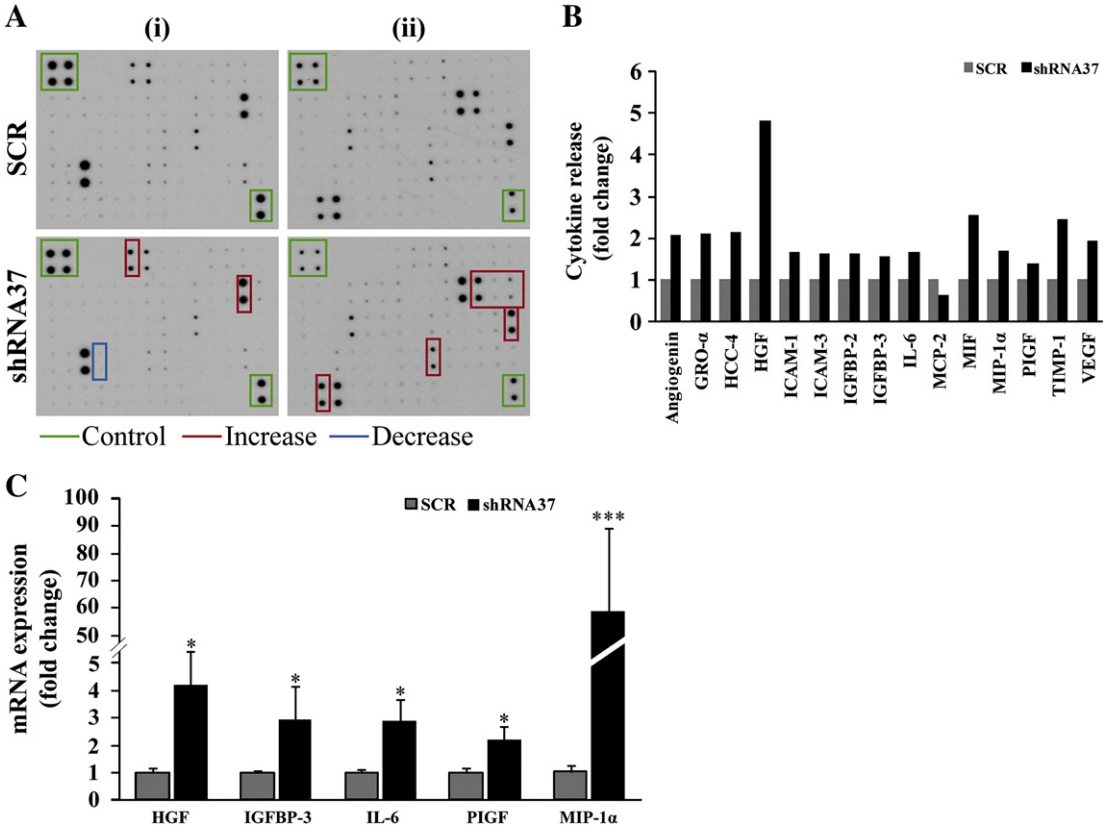

Fig. 5. Cytokine release in Fxn-deficient human astrocyte conditioned medium (ACM). (A) Representative antibody arrays (120 cytokines; i and ii) incubated with ACM (48 h) from the SCR (upper panels) and shRNA37 (lower panels) transduced cells (96 h after transduction). Rectangles indicate the positive controls (green), and some of the up-regulated (red) and down-regulated (blue) cytokines. (B) Bar graph showing the quantification of the cytokines released by shRNA37 transduced HAs (black bars), presented as the fold change with respect to the SCR condition (dark gray bars). (C) Real-time PCR amplification of the HGF, IGFBP-3, IL-6, PlGF and MIP-1α transcripts in SCR (dark gray bars) or Fxn-depleted HAs (black bars) measured 96 h post-transduction. The mRNA expression was quantified by the comparative Ct method and the data are presented as the mean fold change ± S.E.M. from at least three independent samples per experimental condition: $^{*}p < 0.05$ and $^{***}p < 0.001$ compared with SCR.

Table 2
Profile of cytokine release from Fxn-depleted ACM.

Cytokines	Fold increase/decrease
Angiogenesis/proliferation	
Tissue inhibitor of metalloproteinases (TIMP-1)	2.45
Vascular endothelial growth factor A (VEGF-A)	1.93
Angiogenin (ANG)	2.09
Phosphatidylinositol glycan anchor biosynthesis (PIGF)	1.40
Immunity/inflammatory	
Intercellular adhesion molecule 1 (ICAM-1)	1.66
Monocyte Chemotactic Protein 2 (MCP-2)	−1.53
Macrophage migration inhibitory factor (MIF)	2.54
Intercellular adhesion molecule 3 (ICAM-3)	1.64
Growth regulated oncogene-alpha (GRO-α)	2.11
Macrophage inflammatory protein 1 alpha (MIP-1α)	1.72
Chemokine (C–C motif) ligand 16 (HCC-4)	2.14
Broad-acting cytokines	
Interleukin 6 (IL-6)	1.68
Growth factors/binding proteins	
Hepatocyte growth factor (HGF)	4.81
Insulin-like growth factor binding protein 2 (IGFBP-2)	1.64
Insulin-like growth factor binding protein 3 (IGFBP-3)	1.57

Frataxin silencing in human astrocytes alters their capacity to support the development and survival of mouse neurons

One of the main functions of astrocytes is to maintain a healthy environment for neurons by releasing factors that support their growth, development and survival (Sofroniew, 2013). However, they may have a beneficial or detrimental influence on neuronal survival in function of the context (Zamanian et al., 2012; Verkhratsky et al., 2013). To examine the possible functional effects of Fxn depletion in HAs on astrocyte–neuron interactions, we cultured wild-type mouse cortical neurons in the presence of ACM from CTL, SCR or Fxn-deficient HAs (the ACM and wild-type cortical mouse neurons from E17 embryos were prepared as indicated in the Materials and methods section). The plating medium was shifted to ACM 3 h after seeding and the cells were then maintained under these conditions for up to 3 DIV (Fig. 6A), when neurite outgrowth was analyzed by immunocytochemistry with SMI31/MAP-2 and cell viability was quantified by calcein/PI capture and nuclei counts. Subsequent confocal microscopy analysis of SMI31 positive cells revealed that the axons of wild-type neurons grown in CTL-ACM or SCR-ACM lengthened at a normal rate and that the density of the neurons was normal. By contrast, the addition of shRNA37-ACM induced a significant decrease (slightly more than 50%) in axonal branching and neuronal density (Figs. 6B and E). In terms of cell survival, while no significant differences were detected after 2 DIV, the survival of cortical neurons significantly decreased to approximately 60% the control values in the presence of shRNA37-ACM after 3 DIV (Fig. 6C), as confirmed by the total number of DAPI positive cells detected after 3 days in the presence of shRNA37-ACM (Fig. 6D). In addition, we also found that shRNA37-ACM significantly reduced the dendritic arborization of neurons (measured by MAP-2 staining) to approximately 50% that of neurons exposed to CTL and SCR ACM (Fig. 6F). Since these effects occur without any direct contact between astrocytes and neurons, our results suggest that the morphological changes and neuronal death triggered by the ACM from cells lacking Fxn is mediated by one or more soluble factors released by HAs.

Discussion

FA is a multisystemic disease caused by reduced levels of the Fxn protein (Corben et al., 2012). Although its main clinical features involve the degeneration of neurons in the central and peripheral nervous system (Delatycki and Corben, 2012), little is known about the possible contribution of glial cells, and specifically of astrocytes, to the initiation and propagation of this disease. Since astrocytes are the main regulators of brain homeostasis and they have previously been implicated in the pathogenesis of other neurological conditions (Verkhratsky et al., 2012), it appears plausible that the loss of normal astrocyte activity may have negative consequences on glial–neuron interactions in FA.

In this study, an *in vitro* model of Fxn knockdown was established and characterized in human astrocytes. Using this approach, we were able to reduce Fxn protein and mRNA expression to levels similar to those observed under pathological conditions. This Fxn silencing inhibits cell proliferation and induces death of human astrocytes, changes that are accompanied by a significant up-regulation of the tumor suppression protein p53, the cell cycle regulatory protein p21 and the apoptotic marker caspase-3. We also found that as a consequence of Fxn deficiency, the morphology of the mitochondria in these cells is altered and they suffer greater oxidative stress. In addition, we found that Fxn-deficient astrocytes produce a variety of cytokines and growth factors that in turn might influence their capacity to provide trophic support to neurons. Indeed, primary mouse neurons undergo delayed maturation and cell death when cultured in ACM from Fxn-deficient cells.

Since Fxn was first identified, the protein was shown to be strongly expressed in the mitochondria of neurons and astroglia (Campuzano et al., 1997). However, there is little reference in the literature to the expression and function of Fxn in astrocytes (Kirches et al., 2011; Franco et al., 2012). Therefore, our observation of significantly less Fxn protein and mRNA transcripts in human astrocytes several days after *in vitro* knockdown is consistent with our data from neuron-like cells (Palomo et al., 2011) and those from other cell types (Santos et al., 2001; Lu and Cortopassi, 2007; Napoli et al., 2007; Zanella et al., 2008). Interestingly, insulin-like growth factor 1 (IGF-1) can alter Fxn levels in mouse astrocytes and neurons, which suggests that the intrinsic regulation of Fxn is dependent on the cell context (Franco et al., 2012). Curiously, in these studies mouse astrocytes appear to be much less sensitive to Fxn deficiency than neurons, which would appear to contrast with our observations of significant cell death after frataxin depletion in HAs. It remains to be established whether this discrepancy is due to the particular experimental conditions employed or whether it reflects species differences. It is noteworthy that some significant functional differences have been described between mouse and human astrocytes (Oberheim et al., 2009; Tarassishin et al., 2014), and differences in gene expression between murine and human astrocytes might also be responsible for their distinct susceptibility to Fxn depletion. A recent analysis of the transcriptome of the prenatal human brain placed FXN gene within a module enriched for genes expressed in astrocytes (Miller et al., 2014). Clearly, further research is required to clarify this issue.

Astrocytes are considered important regulators of iron homeostasis that become activated under pathological conditions, exerting either beneficial or detrimental effects on the surrounding environment (Tulpule et al., 2010; Pelizzoni et al., 2013). Since Fxn is known to be directly implicated in mitochondrial iron–sulfur cluster biogenesis, the increase in superoxide production and the alterations to mitochondrial morphology after Fxn depletion in astrocytes supports the idea that increasing mitochondrial iron content favors oxidative stress within astroglial cells. Hence, these modifications in their antioxidant defense system might also alter neural homeostasis, an observation confirmed recently in a complex I knockdown model in *Drosophila* that demonstrates the relationship between glial cells and neurotoxicity in the context of mitochondrial electron transport chain disorders (Hegde et al., 2014).

One of the main conclusions drawn after intense research into the functions of Fxn is its involvement in early development and cell survival. The complete deletion of Fxn in mice rapidly provokes embryonic lethality (Cossee et al., 2000), while FA-induced pluripotent stem cells (iPSCs) display deficient differentiation into peripheral sensory neurons (Eigentler et al., 2013). These observations are consistent

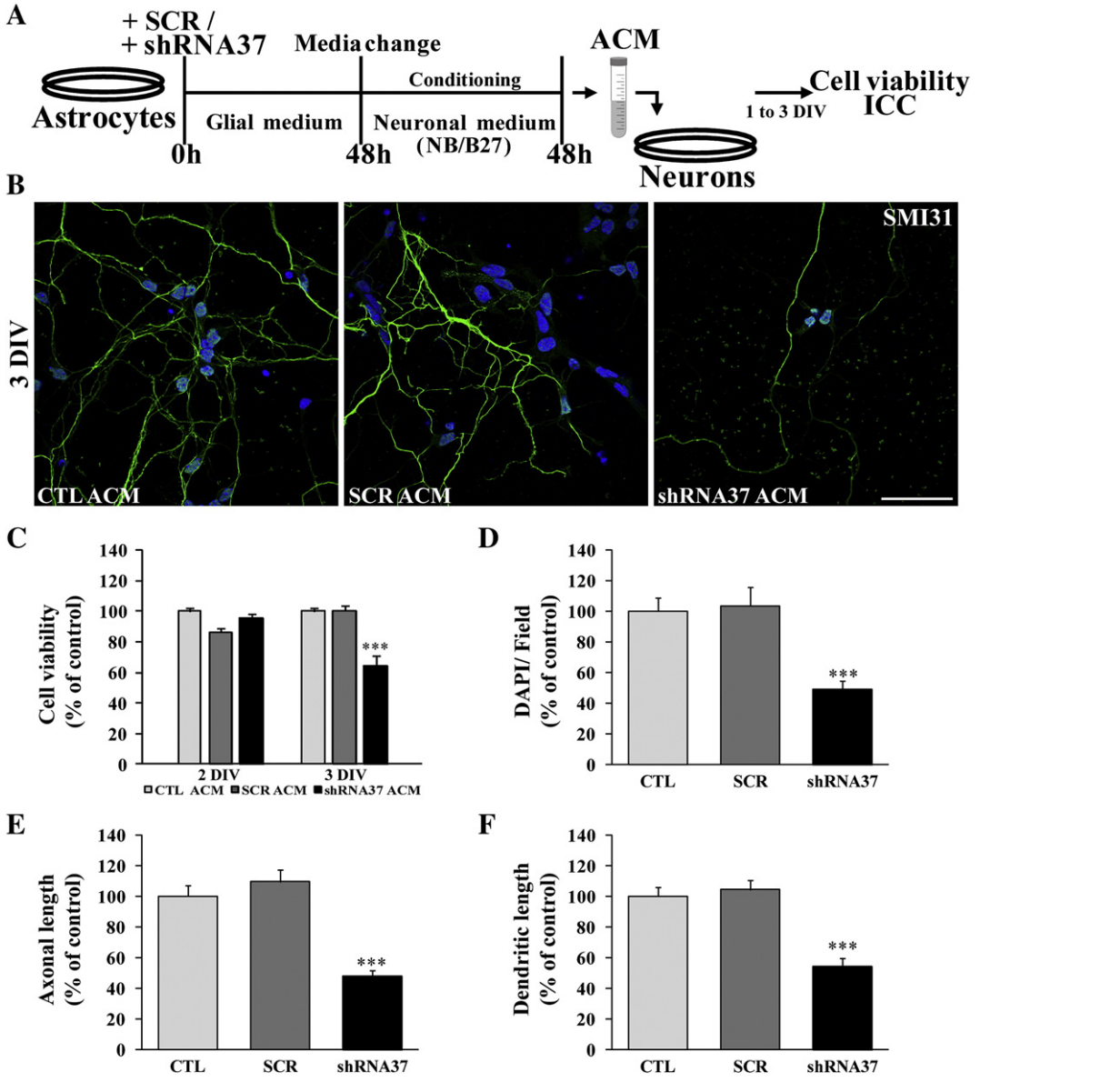

Fig. 6. Conditioned medium from Fxn-depleted HAs (ACM) mediates non-cell autonomous degeneration of wild-type mouse cortical neurons. (A) Scheme of the experimental design and the time line for conditioning HA medium. HA cultures were transduced with SCR, shRNA37 or left untransduced and after 48 h, the medium was replaced with standard neuronal medium for conditioning over a further 48 h (a total of 96 h after lentiviral transduction). (B) Representative confocal photomicrographs of normal mouse cortical neurons grown for 3 days in ACM, having labeled the axons and nuclei with anti-SMI31 (green) and DAPI (blue), respectively. Scale bar: 50 μm. (C–F) Neuron viability, total cell number and neurite length (SMI31 and MAP-2 positive cells) were measured after 2 or 3 days in the presence of CTL-ACM (light gray bar), SCR-ACM (dark gray bar) or shRNA37-ACM (black bar). (C and D) Cell viability and the total cell number were evaluated by the calcein/PI assay and DAPI counts. (E and F) Axonal and dendritic lengths were calculated using the NeuronJ plugin of the ImageJ software (as described elsewhere). The data represent the mean ± S.E.M. of three independent experiments, presented as percentage of the CTL condition: $^{***}p < 0.001$ compared with SCR.

with results from models in which susceptibility to neurodegeneration and cell death is enhanced when Fxn levels are reduced. However, the mechanisms by which Fxn depletion induces these alterations are not yet fully understood. In our hands, human cortical astrocyte survival is significantly compromised as a consequence of the lack of Fxn, a similar finding to that reported in rat dorsal root ganglia (Mincheva-Tasheva et al., 2014) and in Schwann cells (Lu et al., 2009). Interestingly, we observe a correlation between astrocyte cell death and activation of the p53 pathway. The relationship between p53 and glial cells in a pathological context has been poorly studied until recently, and the evidence emerging suggests a contribution of astrocytic p53 to some neurodegenerative diseases (for review see Jebelli et al., 2012). Our results support the idea that p53 is important in the response to Fxn depletion, not only in neurons (Palomo et al., 2011) but also in glial cells. However, the precise interaction between Fxn expression and p53 signaling may also depend on cell context and thus become rather complex. For instance, immortalized B lymphoblasts from FA patients exhibit increased basal levels of phosphorylated p53 but a less efficient activation of p53 upon hypoxia (Guccini et al., 2011). This differential modulation of p53 activation by Fxn expression level in normoxia and hypoxia might also lead to a differential recruitment of distinct p53 downstream targets (Guccini et al., 2011). On the other hand, it has been recently described that p53 activates the transcription of the FXN gene in a human embryonic kidney cell line (Shimizu et al., 2014). Further research is necessary to clarify the complex interrelationship between Fxn and p53 in distinct cell types under different physiopathological conditions.

Given that some important astrocyte functions are mediated by the release of different molecules, we analyzed the secretome of human astrocytes in our *in vitro* model. Astrocyte secretomes have already been investigated in health and disease using a range of techniques (Lafon-Cazal et al., 2003; Pocernich et al., 2005; Jha et al., 2013; Lai et al., 2013). Our cytokine screening and validation through mRNA

expression identified alterations in the cytokine composition of the ACM of Fxn-depleted astrocytes, mainly those associated with processes like immunity, inflammation and/or proliferation. Among the up-regulated molecules, IL-6 has often been considered a potent pro-inflammatory mediator produced by glial cells in response to various types of insults. This up-regulation is consistent with that described previously when Fxn is silenced in Schwann cell lines (Lu et al., 2009) and thus, IL-6 up-regulation may represent a general glial response to Fxn deficiency regulating inflammation. Interestingly, an increased secretion of IL-6 has also been reported to occur after persistent DNA damage (Rodier et al., 2009) and may be considered one of the factors linking oxidative stress and inflammation. Likewise, the increased expression of the chemokine MIP-1α, which is also involved in the regulation of inflammatory processes, is consistent with its expression in reactive astrocytes (Murphy et al., 1995; Di Malta et al., 2012).

The up-regulation of HGF, a potent growth factor with pleiotropic activity related to tissue protection and regeneration that is enhanced in reactive astrocytes *in vivo*, is particularly relevant (Shimamura et al., 2007; Nakamura et al., 2011; Jeong et al., 2012). Since astrocytes exert beneficial effects by regulating local immune responses, the increased expression of this molecule by these cells when Fxn is lacking suggests that a physiological compensatory mechanism may be triggered to protect them.

The importance of studying the glial contribution to FA has been emphasized in a model of the disease in which the specific deletion of glial Fxn in *Drosophila* generated FA-like symptoms, including a reduced lifespan, increased sensitivity to oxidative insults and impaired locomotor activity (Navarro et al., 2010). Here we show that the ACM from Fxn-knockdown cortical astrocytes is sufficient to elicit a neurodegenerative phenotype in cortical neurons from wild-type mice, characterized by a high rate of cell death and a reduction in neurite length. Given the altered levels of some cytokines and growth factors detected in the ACM, the release of these molecules might be at least partially responsible for the non-cell autonomous detrimental effects observed, although astrocytes may induce neurodegeneration in FA through other mechanisms. Nevertheless, our results support the hypothesis that astrocytes may become neurotoxic in FA, as proposed in other neurological diseases. The toxic effects of astrocytes differentiated from Rett syndrome iPSCs on the morphology and function of mouse hippocampal neurons has recently been demonstrated *in vitro*, and similar results were obtained with ACM, highlighting the non-cell autonomous mechanisms implicated in this neurological syndrome (Williams et al., 2014). Along similar lines, the conditional deletion of the Dicer endoribonuclease in astrocytes *in vivo* causes a wide range of neurological alterations and premature death in mice (Tao et al., 2011), and neurodegeneration was described in an astrocyte conditioned mouse model of multiple sulfatase deficiency (Di Malta et al., 2012). Evidence of non-cell autonomous toxicity of wild-type motor neurons was also obtained in a co-culture system with neuronal progenitor cell-derived astrocytes from patients with amyotrophic lateral sclerosis (Meyer et al., 2014).

In conjunction with the *Drosophila* model of glial-specific Fxn depletion (Navarro et al., 2010), our cell model of Fxn deficiency in human astrocytes further suggests that non-cell-autonomous neurodegeneration may contribute to the pathogenesis of FA. However, this work is limited by the differences that might exist between *in vitro*/*in vivo* approaches to study the role of astrocytes in the progression of neurodegenerative pathologies (Cahoy et al., 2008), as well as by the heterogeneity among astrocytes, not only in terms of morphology but also functionally, and/or in their capacity to respond to injury (for review see Zhang and Barres, 2010). A complementary approach would be to investigate the possible contribution of glial cells to the initiation or progression of the disease directly through the generation of novel conditional mouse models of Fxn deficiency (Perdomini et al., 2013).

Interestingly, some recent evidence supports the hypothesis that neuroinflammation may be a contributing factor to the pathogenesis of FA (Hayashi et al., 2014). An up-regulation of inducible cyclooxygenase 2 (COX-2) and an increased biosynthesis of prostanoids have been observed in two FA mouse models as well as in lymphocytes from FA patients (Hayashi et al., 2014). In the discussion of their findings, Hayashi and colleagues suggest that the chronic elevation of oxidative stress in FA patient cells and animal models may lead to the secretion of cytokines responsible for COX-2 up-regulation. These authors have proposed a mechanism involving Fxn-deficit → Oxidative stress → Cytokines → COX-2 → Neuroinflammation → Neurodegeneration (Hayashi et al., 2014). Our results agree well with this model and emphasize the role played by astrocytes in this respect, suggesting a mechanism involving Fxn-deficit-in-glia → Oxidative stress → Cytokines → Neuroinflammation → Neurodegeneration.

Further research both in animal models and in the clinical setting is required to investigate the role of neuroinflammation in the physiopathology of FA. Of interest in this regard is the observation of a significant telomere shortening in the peripheral blood leukocytes from FA patients compared with healthy subjects (Castaldo et al., 2013), as it has been suggested that increased telomere attrition may be caused by oxidative stress and inflammation (Eitan et al., 2014). Moreover, the possible occurrence of demyelination in FA patients (Corben et al., 2014) may be associated with mitochondrial dysfunction, oxidative stress and neuroinflammation (Carvalho, 2013).

Astrocytes also play important roles in supporting the development and maintenance of CNS myelin (Barnett and Linington, 2013). In fact, dysfunctional astrocytes may negatively affect oligodendrocytes, as observed in a number of diseases in which astrocytic pathology is known as the direct cause of myelin pathology (Brosnan and Raine, 2013; Clemente et al., 2013; Lundgaard et al., 2014). Thus, we may also speculate with the possibility that the up-regulation of pro-inflammatory cytokines in Fxn-deficient astrocytes leads to the demyelination observed in FA (Corben et al., 2014).

In summary, our results favor the view that Fxn-deficient astrocytes may contribute to neuropathology in FA through non-cell autonomous processes including neuroinflammation.

Financial interests or conflicts

None.

Acknowledgments

This work was supported by a grant from the "l'Association Française de l'Ataxie de Friedreich" (AFAF), as well as the Spanish National Research Plan (SAF 2012-38042) and the Autonomous Government of Madrid (S20/BMD-2331). The Center for Biomedical Research on Rare Diseases ("Centro de Investigación Biomédica en Red sobre Enfermedades Raras", CIBERER) is an initiative supported by the "Instituto de Salud Carlos III".

References

Allaman, I., Belanger, M., Magistretti, P.J., 2011. Astrocyte–neuron metabolic relationships: for better and for worse. Trends Neurosci. 34, 76–87.
Aurelie, D., Carole, E., Nicole, D., 2013. Lentiviral vectors: a powerful tool to target astrocytes *in vivo*. Curr. Drug Targets 14, 1336–1346.
Barnett, S.C., Linington, C., 2013. Myelination: do astrocytes play a role? Neuroscientist 19, 442–450.
Barres, B.A., 2008. The mystery and magic of glia: a perspective on their roles in health and disease. Neuron 60, 430–440.
Belanger, M., Allaman, I., Magistretti, P.J., 2011. Brain energy metabolism: focus on astrocyte–neuron metabolic cooperation. Cell Metab. 14, 724–738.
Brosnan, C.F., Raine, C.S., 2013. The astrocyte in multiple sclerosis revisited. Glia 61, 453–465.
Cahoy, J.D., Emery, B., Kaushal, A., Foo, L.C., Zamanian, J.L., Christopherson, K.S., Xing, Y., Lubischer, J.L., Krieg, P.A., Krupenko, S.A., Thompson, W.J., Barres, B.A., 2008. A transcriptome database for astrocytes, neurons, and oligodendrocytes: a new resource for understanding brain development and function. J. Neurosci. 28, 264–278.
Campuzano, V., Montermini, L., Molto, M.D., Pianese, L., Cossee, M., Cavalcanti, F., Monros, E., Rodius, F., Duclos, F., Monticelli, A., Zara, F., Canizares, J., Koutnikova, H., Bidichandani, S.I., Gellera, C., Brice, A., Trouillas, P., De Michele, G., Filla, A., De Frutos, R., Palau, F., Patel, P.I., Di Donato, S., Mandel, J.L., Cocozza, S., Koenig, M.,

Pandolfo, M., 1996. Friedreich's ataxia: autosomal recessive disease caused by an intronic GAA triplet repeat expansion. Science (New York, N.Y.) 271, 1423–1427.
Campuzano, V., Montermini, L., Lutz, Y., Cova, L., Hindelang, C., Jiralerspong, S., Trottier, Y., Kish, S.J., Faucheux, B., Trouillas, P., Authier, F.J., Durr, A., Mandel, J.L., Vescovi, A., Pandolfo, M., Koenig, M., 1997. Frataxin is reduced in Friedreich ataxia patients and is associated with mitochondrial membranes. Hum. Mol. Genet. 6, 1771–1780.
Carvalho, K.S., 2013. Mitochondrial dysfunction in demyelinating diseases. Semin. Pediatr. Neurol. 20, 194–201.
Castaldo, I., Vergara, P., Pinelli, M., Filla, A., De Michele, G., Cocozza, S., Monticelli, A., 2013. Can telomere shortening in human peripheral blood leukocytes serve as a disease biomarker of Friedreich's ataxia? Antioxid. Redox Signal. 18, 1303–1306.
Clemente, D., Ortega, M.C., Melero-Jerez, C., de Castro, F., 2013. The effect of glia–glia interactions on oligodendrocyte precursor cell biology during development and in demyelinating diseases. Front. Cell. Neurosci. 7, 268.
Corben, L.A., Georgiou-Karistianis, N., Bradshaw, J.L., Evans-Galea, M.V., Churchyard, A.J., Delatycki, M.B., 2012. Characterising the neuropathology and neurobehavioural phenotype in Friedreich ataxia: a systematic review. Adv. Exp. Med. Biol. 769, 169–184.
Corben, L.A., Kashuk, S.R., Akhlaghi, H., Jamadar, S., Delatycki, M.B., Fielding, J., Johnson, B., Georgiou-Karistianis, N., Egan, G.F., 2014. Myelin paucity of the superior cerebellar peduncle in individuals with Friedreich ataxia: an MRI magnetization transfer imaging study. J. Neurol. Sci. 343, 138–143.
Cossee, M., Puccio, H., Gansmuller, A., Koutnikova, H., Dierich, A., LeMeur, M., Fischbeck, K., Dolle, P., Koenig, M., 2000. Inactivation of the Friedreich ataxia mouse gene leads to early embryonic lethality without iron accumulation. Hum. Mol. Genet. 9, 1219–1226.
Delatycki, M.B., Corben, L.A., 2012. Clinical features of Friedreich ataxia. J. Child Neurol. 27, 1133–1137.
Di Malta, C., Fryer, J.D., Settembre, C., Ballabio, A., 2012. Astrocyte dysfunction triggers neurodegeneration in a lysosomal storage disorder. Proc. Natl. Acad. Sci. U. S. A. 109, E2334–2342.
Dowling, P., Clynes, M., 2011. Conditioned media from cell lines: a complementary model to clinical specimens for the discovery of disease-specific biomarkers. Proteomics 11, 794–804.
Eigentler, A., Boesch, S., Schneider, R., Dechant, G., Nat, R., 2013. Induced pluripotent stem cells from friedreich ataxia patients fail to upregulate frataxin during *in vitro* differentiation to peripheral sensory neurons. Stem Cells Dev. 22, 3271–3282.
Eitan, E., Hutchison, E.R., Mattson, M.P., 2014. Telomere shortening in neurological disorders: an abundance of unanswered questions. Trends Neurosci. 37, 256–263.
Follenzi, A., Naldini, L., 2002. HIV-based vectors. Preparation and use. Methods Mol Med 69, 259–274.
Franco, C., Fernandez, S., Torres-Aleman, I., 2012. Frataxin deficiency unveils cell-context dependent actions of insulin-like growth factor I on neurons. Mol. Neurodegener. 7, 51.
Garden, G.A., La Spada, A.R., 2012. Intercellular (mis)communication in neurodegenerative disease. Neuron 73, 886–901.
Gonzalez-Cabo, P., Palau, F., 2013. Mitochondrial pathophysiology in Friedreich's ataxia. J. Neurochem. 126 (Suppl. 1), 53–64.
Guccini, I., Serio, D., Condo, I., Rufini, A., Tomassini, B., Mangiola, A., Maira, G., Anile, C., Fina, D., Pallone, F., Mongiardi, M.P., Levi, A., Ventura, N., Testi, R., Malisan, F., 2011. Frataxin participates to the hypoxia-induced response in tumors. Cell Death Dis 2, e123.
Hayashi, G., Shen, Y., Pedersen, T.L., Newman, J.W., Pook, M., Cortopassi, G., 2014. Frataxin deficiency increases cyclooxygenase 2 and prostaglandins in cell and animal models of Friedreich's ataxia. Hum. Mol. Genet. 23, 6838–6847.
Hegde, V.R., Vogel, R., Feany, M.B., 2014. Glia are critical for the neuropathology of complex I deficiency in *Drosophila*. Hum. Mol. Genet. 23, 4686–4692.
Ilieva, H., Polymenidou, M., Cleveland, D.W., 2009. Non-cell autonomous toxicity in neurodegenerative disorders: ALS and beyond. J. Cell Biol. 187, 761–772.
Jebelli, J.D., Hooper, C., Garden, G.A., Pocock, J.M., 2012. Emerging roles of p53 in glial cell function in health and disease. Glia 60, 515–525.
Jeong, S.R., Kwon, M.J., Lee, H.G., Joe, E.H., Lee, J.H., Kim, S.S., Suh-Kim, H., Kim, B.G., 2012. Hepatocyte growth factor reduces astrocytic scar formation and promotes axonal growth beyond glial scars after spinal cord injury. Exp. Neurol. 233, 312–322.
Jha, M.K., Seo, M., Kim, J.H., Kim, B.G., Cho, J.Y., Suk, K., 2013. The secretome signature of reactive glial cells and its pathological implications. Biochim. Biophys. Acta 1834, 2418–2428.
Kirches, E., Andrae, N., Hoefer, A., Kehler, B., Zarse, K., Leverkus, M., Keilhoff, G., Schonfeld, P., Schneider, T., Wilisch-Neumann, A., Mawrin, C., 2011. Dual role of the mitochondrial protein frataxin in astrocytic tumors. Lab Invest 91, 1766–1776.
Koeppen, A.H., Mazurkiewicz, J.E., 2013. Friedreich ataxia: neuropathology revised. J. Neuropathol. Exp. Neurol. 72, 78–90.
Lafon-Cazal, M., Adjali, O., Galeotti, N., Poncet, J., Jouin, P., Homburger, V., Bockaert, J., Marin, P., 2003. Proteomic analysis of astrocytic secretion in the mouse. Comparison with the cerebrospinal fluid proteome. J Biol Chem 278, 24438–24448.
Lai, W., Wu, J., Zou, X., Xie, J., Zhang, L., Zhao, X., Zhao, M., Wang, Q., Ji, J., 2013. Secretome analyses of Abeta(1–42) stimulated hippocampal astrocytes reveal that CXCL10 is involved in astrocyte migration. J. Proteome Res. 12, 832–843.
Laurell, H., Iacovoni, J.S., Abot, A., Svec, D., Maoret, J.J., Arnal, J.F., Kubista, M., 2012. Correction of RT-qPCR data for genomic DNA-derived signals with ValidPrime. Nucleic Acids Res. 40, e51.
Lefevre, S., Sliwa, D., Rustin, P., Camadro, J.M., Santos, R., 2012. Oxidative stress induces mitochondrial fragmentation in frataxin-deficient cells. Biochem. Biophys. Res. Commun. 418, 336–341.
Liu, N., Stoica, G., Yan, M., Scofield, V.L., Qiang, W., Lynn, W.S., Wong, P.K., 2005. ATM deficiency induces oxidative stress and endoplasmic reticulum stress in astrocytes. Lab Invest 85, 1471–1480.
Loria, F., Petrosino, S., Hernangomez, M., Mestre, L., Spagnolo, A., Correa, F., Di Marzo, V., Docagne, F., Guaza, C., 2010. An endocannabinoid tone limits excitotoxicity *in vitro* and in a model of multiple sclerosis. Neurobiol. Dis. 37, 166–176.
Lu, C., Cortopassi, G., 2007. Frataxin knockdown causes loss of cytoplasmic iron–sulfur cluster functions, redox alterations and induction of heme transcripts. Arch. Biochem. Biophys. 457, 111–122.
Lu, C., Schoenfeld, R., Shan, Y., Tsai, H.J., Hammock, B., Cortopassi, G., 2009. Frataxin deficiency induces Schwann cell inflammation and death. Biochim. Biophys. Acta 1792, 1052–1061.
Lundgaard, I., Osorio, M.J., Kress, B.T., Sanggaard, S., Nedergaard, M., 2014. White matter astrocytes in health and disease. Neuroscience 276, 161–173.
Mattson, M.P., Barger, S.W., Begley, J.G., Mark, R.J., 1995. Calcium, free radicals, and excitotoxic neuronal death in primary cell culture. Methods Cell Biol. 46, 187–216.
Meijering, E., Jacob, M., Sarria, J.C., Steiner, P., Hirling, H., Unser, M., 2004. Design and validation of a tool for neurite tracing and analysis in fluorescence microscopy images. Cytometry A 58, 167–176.
Meyer, K., Ferraiuolo, L., Miranda, C.J., Likhite, S., McElroy, S., Renusch, S., Ditsworth, D., Lagier-Tourenne, C., Smith, R.A., Ravits, J., Burghes, A.H., Shaw, P.J., Cleveland, D.W., Kolb, S.J., Kaspar, B.K., 2014. Direct conversion of patient fibroblasts demonstrates non-cell autonomous toxicity of astrocytes to motor neurons in familial and sporadic ALS. Proc. Natl. Acad. Sci. U. S. A. 111, 829–832.
Miller, J.A., Ding, S.L., Sunkin, S.M., Smith, K.A., Ng, L., Szafer, A., Ebbert, A., Riley, Z.L., Royall, J.J., Aiona, K., Arnold, J.M., Bennet, C., Bertagnolli, D., Brouner, K., Butler, S., Caldejon, S., Carey, A., Cuhaciyan, C., Dalley, R.A., Dee, N., Dolbeare, T.A., Facer, B.A., Feng, D., Fliss, T.P., Gee, G., Goldy, J., Gourley, L., Gregor, B.W., Gu, G., Howard, R.E., Jochim, J.M., Kuan, C.L., Lau, C., Lee, C.K., Lee, F., Lemon, T.A., Lesnar, P., McMurray, B., Mastan, N., Mosqueda, N., Naluai-Cecchini, T., Ngo, N.K., Nyhus, J., Oldre, A., Olson, E., Parente, J., Parker, P.D., Parry, S.E., Stevens, A., Pletikos, M., Reding, M., Roll, K., Sandman, D., Sarreal, M., Shapouri, S., Shapovalova, N.V., Shen, E.H., Sjoquist, N., Slaughterbeck, C.R., Smith, M., Sodt, A.J., Williams, D., Zollei, L., Fischl, B., Gerstein, M.B., Geschwind, D.H., Glass, I.A., Hawrylycz, M.J., Hevner, R.F., Huang, H., Jones, A.R., Knowles, J.A., Levitt, P., Phillips, J.W., Sestan, N., Wohnoutka, P., Dang, C., Bernard, A., Hohmann, J.G., Lein, E.S., 2014. Transcriptional landscape of the prenatal human brain. Nature 508, 199–206.
Mincheva-Tasheva, S., Obis, E., Tamarit, J., Ros, J., 2014. Apoptotic cell death and altered calcium homeostasis caused by frataxin depletion in dorsal root ganglia neurons can be prevented by BH4 domain of Bcl-xL protein. Hum. Mol. Genet. 23, 1829–1841.
Mukhopadhyay, P., Rajesh, M., Hasko, G., Hawkins, B.J., Madesh, M., Pacher, P., 2007. Simultaneous detection of apoptosis and mitochondrial superoxide production in live cells by flow cytometry and confocal microscopy. Nat. Protoc. 2, 2295–2301.
Murphy Jr., G.M., Jia, X.C., Song, Y., Ong, E., Shrivastava, R., Bocchini, V., Lee, Y.L., Eng, L.F., 1995. Macrophage inflammatory protein 1-alpha mRNA expression in an immortalized microglial cell line and cortical astrocyte cultures. J. Neurosci. Res. 40, 755–763.
Nakamura, T., Sakai, K., Nakamura, T., Matsumoto, K., 2011. Hepatocyte growth factor twenty years on: Much more than a growth factor. J. Gastroenterol. Hepatol. 26 (Suppl. 1), 188–202.
Napoli, E., Morin, D., Bernhardt, R., Buckpitt, A., Cortopassi, G., 2007. Hemin rescues adrenodoxin, heme a and cytochrome oxidase activity in frataxin-deficient oligodendroglioma cells. Biochim. Biophys. Acta 1772, 773–780.
Navarro, J.A., Ohmann, E., Sanchez, D., Botella, J.A., Liebisch, G., Molto, M.D., Ganfornina, M.D., Schmitz, G., Schneuwly, S., 2010. Altered lipid metabolism in a *Drosophila* model of Friedreich's ataxia. Hum. Mol. Genet. 19, 2828–2840.
Oberheim, N.A., Takano, T., Han, X., He, W., Lin, J.H., Wang, F., Xu, Q., Wyatt, J.D., Pilcher, W., Ojemann, J.G., Ransom, B.R., Goldman, S.A., Nedergaard, M., 2009. Uniquely hominid features of adult human astrocytes. J. Neurosci. 29, 3276–3287.
Palomo, G.M., Cerrato, T., Gargini, R., Diaz-Nido, J., 2011. Silencing of frataxin gene expression triggers p53-dependent apoptosis in human neuron-like cells. Hum. Mol. Genet. 20, 2807–2822.
Pastore, A., Puccio, H., 2013. Frataxin: a protein in search for a function. J. Neurochem. 126 (Suppl. 1), 43–52.
Pelizzoni, I., Zacchetti, D., Campanella, A., Grohovaz, F., Codazzi, F., 2013. Iron uptake in quiescent and inflammation-activated astrocytes: a potentially neuroprotective control of iron burden. Biochim. Biophys. Acta 1832, 1326–1333.
Perdomini, M., Hick, A., Puccio, H., Pook, M.A., 2013. Animal and cellular models of Friedreich ataxia. J. Neurochem. 126 (Suppl. 1), 65–79.
Pocernich, C.B., Boyd-Kimball, D., Poon, H.F., Thongboonkerd, V., Lynn, B.C., Klein, J.B., Calebrese, V., Nath, A., Butterfield, D.A., 2005. Proteomics analysis of human astrocytes expressing the HIV protein Tat. Brain Res. Mol. Brain Res. 133, 307–316.
Rodier, F., Coppe, J.P., Patil, C.K., Hoeijmakers, W.A., Munoz, D.P., Raza, S.R., Freund, A., Campeau, E., Davalos, A.R., Campisi, J., 2009. Persistent DNA damage signalling triggers senescence-associated inflammatory cytokine secretion. Nat. Cell Biol. 11, 973–979.
Rodriguez, J.J., Verkhratsky, A., 2011. Neuroglial roots of neurodegenerative diseases? Mol. Neurobiol. 43, 87–96.
Sanchez Martin, C., Diaz-Nido, J., Avila, J., 1998. Regulation of a site-specific phosphorylation of the microtubule-associated protein 2 during the development of cultured neurons. Neuroscience 87, 861–870.
Santos, M.M., Ohshima, K., Pandolfo, M., 2001. Frataxin deficiency enhances apoptosis in cells differentiating into neuroectoderm. Hum. Mol. Genet. 10, 1935–1944.
Shimamura, M., Sato, N., Sata, M., Wakayama, K., Ogihara, T., Morishita, R., 2007. Expression of hepatocyte growth factor and c-Met after spinal cord injury in rats. Brain Res. 1151, 188–194.
Shimizu, R., Lan, N.N., Tai, T.T., Adachi, Y., Kawazoe, A., Mu, A., Taketani, S., 2014. p53 directly regulates the transcription of the human frataxin gene and its lack of regulation in tumor cells decreases the utilization of mitochondrial iron. Gene 551, 79–85.

Sofroniew, M.V., 2013. Multiple roles for astrocytes as effectors of cytokines and inflammatory mediators. Neuroscientist 20, 160–172.
Sofroniew, M.V., Vinters, H.V., 2010. Astrocytes: biology and pathology. Acta Neuropathol. 119, 7–35.
Tao, J., Wu, H., Lin, Q., Wei, W., Lu, X.H., Cantle, J.P., Ao, Y., Olsen, R.W., Yang, X.W., Mody, I., Sofroniew, M.V., Sun, Y.E., 2011. Deletion of astroglial Dicer causes non-cell-autonomous neuronal dysfunction and degeneration. J. Neurosci. 31, 8306–8319.
Tapia, M., Wandosell, F., Garrido, J.J., 2010. Impaired function of HDAC6 slows down axonal growth and interferes with axon initial segment development. PLoS One 5, e12908.
Tarassishin, L., Suh, H.S., Lee, S.C., 2014. LPS and IL-1 differentially activate mouse and human astrocytes: role of CD14. Glia 62, 999–1013.
Tulpule, K., Robinson, S.R., Bishop, G.M., Dringen, R., 2010. Uptake of ferrous iron by cultured rat astrocytes. J. Neurosci. Res. 88, 563–571.
Verkhratsky, A., Sofroniew, M.V., Messing, A., deLanerolle, N.C., Rempe, D., Rodriguez, J.J., Nedergaard, M., 2012. Neurological diseases as primary gliopathies: a reassessment of neurocentrism. ASN Neuro 4.
Verkhratsky, A., Rodriguez, J.J., Parpura, V., 2013. Astroglia in neurological diseases. Future Neurol. 8, 149–158.
Williams, E.C., Zhong, X., Mohamed, A., Li, R., Liu, Y., Dong, Q., Ananiev, G.E., Mok, J.C., Lin, B.R., Lu, J., Chiao, C., Cherney, R., Li, H., Zhang, S.C., Chang, Q., 2014. Mutant astrocytes differentiated from Rett syndrome patients-specific iPSCs have adverse effects on wild-type neurons. Hum. Mol. Genet. 23, 2968–2980.
Zamanian, J.L., Xu, L., Foo, L.C., Nouri, N., Zhou, L., Giffard, R.G., Barres, B.A., 2012. Genomic analysis of reactive astrogliosis. J. Neurosci. 32, 6391–6410.
Zanella, I., Derosas, M., Corrado, M., Cocco, E., Cavadini, P., Biasiotto, G., Poli, M., Verardi, R., Arosio, P., 2008. The effects of frataxin silencing in HeLa cells are rescued by the expression of human mitochondrial ferritin. Biochim. Biophys. Acta 1782, 90–98.
Zhang, Y., Barres, B.A., 2010. Astrocyte heterogeneity: an underappreciated topic in neurobiology. Curr. Opin. Neurobiol. 20, 588–594.